Atomic structure and Electronic structure of disordered Graphitic Carbon Nitride

Haichang Lu[1], Yuzheng Guo[2], Jacob W Martin[3,4], Markus Kraft[3,4], John Robertson[1]*

[1]Department of Engineering, Cambridge University, Cambridge CB3 0FA, United Kingdom
[2]School of Engineering, Swansea University, Swansea, SA1 8EN, UK
[3]Dept of Chemical Engineering and Biotechnology, Cambridge University CB2 3RA, UK,
[4] C4T CREATE, National Research Foundation, CREATE Tower, 138602 Singapore.

- jr@eng.cam.ac.uk

Abstract Random networks of sp^2 bonded amorphous graphitic carbon nitride (g-CN) have been created by density functional molecular dynamics calculations. A direct molecular dynamics approach was found to create a network with too many like-atom bonds so that an indirect method via an h-BN random network is used. The resulting network possesses the local units of melems found in the crystalline g-C_3N_4 lattice. The networks have the electron affinity and ionization potential values compatible with photocatalytic water splitting. They are found to possess too many defects so that the band gap is smaller than found experimentally.

1 Introduction

The materials requirements for photocatalytic (PC) water splitting differ from those for photovoltaic (PV) cells. For PV, the main requirement is that the energy gap should match the peak of the solar spectrum. For PC, the band gap should not only match the solar spectrum, but the average band energies referred to the vacuum level (electron affinity and ionization potential) should also match the electrode potentials of the hydrogen and oxygen evolution reactions. In addition, the photocatalyst should be stable in the water against oxidation or reaction.

An early example of TiO_2 as a photocatalyst shows the problem [1]. It is reasonably stable in water, but its band gap is too large, and its band energies lie too far below the vacuum level for it to be an efficient photocatalyst [2]. Indeed, most metal oxides have band edge energies that are too deep below the vacuum level because of the high electronegativity of oxygen.

Of the binary semiconductors, it was noted that the band energies of (In, Ga)N alloys can be tuned to match the requirements for water splitting [3]. This is because nitrogen is less electronegative than oxygen so that the band energies of nitrides lie higher than those of oxides. However, nitrides are less stable and can be oxidized in contact with water. Also, (In,Ga) nitrides have the disadvantage of needing a costly chemical vapor deposition process.

There is however one nitride which can satisfy these conditions, graphitic carbon nitride or g-CN_x [4]. It has a reasonable band gap, and its average electronegativity allows its band energies to be

suitably deep but not too deep below the vacuum level. Also, being a nitride of a first-row element, it has greater thermodynamic stability than other nitrides and so is stable against oxidation. Thirdly, it consists of earth-abundant elements. A final valuable property is to have catalytic activity for the oxygen evolution or hydrogen evolution reactions, but for this CN_x may be require additional components, which is beyond the scope of this work.

Graphitic CN_x is a polymeric compound formed by the condensation of melamine, urea or similar species. The ideal compound has a planar structure like graphene itself. Both the C and N sites are sp^2 bonded, although 75% of the nitrogen are 2-fold coordinated. It is a π-conjugated semiconductor. Although g-CN_x is now well known to the chemical community [4-18], previously there was great interest in a hypothetical sp^3 bonded C_3N_4, which was calculated to be harder than diamond [19]. This form of C_3N_4 has saturated bonding, with carbon as sp^3 and nitrogen as 3-fold coordinated, as in β-Si_3N_4. This 'diamond-like' CN_x would be formed as a thin film by an ion-beam deposition process [20,21] but in practice, it never achieves a high diamond-like fraction.

Returning to g-C_3N_4, a disadvantage of the ideal g-C_3N_4 compound is that its band gap is larger than optimum for the solar spectrum, resulting in a lower conversion efficiency. It was found that the controlled addition of nitrogen vacancies into the structure would reduce the effective band gap, and so bring it closer to the optimum for the solar spectrum [16]. An alternative is to use an amorphous network which would have a smaller band gap [9]. However, there has been less analysis of the effects of disorder on the electronic structure of g-CN_x. This is important as g-CN_x does not have such high carrier mobility [10]. Also, sp^2 bonded lattices can be strongly affected by the disorder, in that the electronic π states can be strongly localized [22]. The first need is to construct a disordered g-C_3N_4 network, containing both the medium range order of tri-s-triazine (melem) units and longer range order.

In this paper, we first describe the character of the various electronic states across the energy spectrum for the crystalline g-C_3N_4 lattice. We then describe how to create amorphous g-C_3N_4 random networks and then calculate their electronic states. The creation of the random networks draws on recent work on the creation of random networks of sp^2 glassy carbon. There are well-established procedures for the creation of random networks of σ bonded systems of sp^3 a-Si or a-C [23-27]. These interact via bond-stretching and bond-bending force fields, giving rise to short range order. Thus their random networks possess mostly short-range order. On the other hand, it was realized that sp^2 a-C requires a medium range order (MRO) of paired sites and 6-fold graphitic rings, in order for the system to possess its observed band gap [28,29]. Such networks with MRO require much larger building blocks to be described properly, and thus much larger supercells to describe their periodicity [30-34]. Glassy carbon requires the largest networks. The techniques to

build networks for this case have only recently become available, mostly using reactive force fields [30-32]. An idea of the necessary dimensions can be seen from the lattice constants of periodic structures of sp^2 sites, as seen in the negative curvature solids [35].

2 Methods

We use primarily the CASTEP plane-wave density functional theory (DFT) code [36] for the periodic supercell models of amorphous carbon (a-C) and amorphous carbon nitride (a-CN_x). Ultra-soft pseudopotentials are used. For the calculation of g-C_3N_4, a vacuum of 30Å is used to simulate a 2D structure. For molecular dynamics of a-C, we use local-density approximation (LDA) as the exchange-correlation functional. The energy cut-off is set to 200 eV to save computation time. For the subsequent geometry optimization, we use the Perdew-Burke-Ernzerhof (PBE) form of the generalized gradient approximation (GGA) as exchange-correlation functional. The cut-off energy is 280 eV. All atomic structures are relaxed to a residual force of less than 0.03 eV/Å. Generally, LDA and GGA underestimate the band gap of semiconductors and insulators. Therefore, we use the Heyd-Scuseria-Ernzerhof (HSE) hybrid functional to calculate the electronic properties [37]. The HSE parameters α and ω are set to 0.2 as in HSE06 to give a better band gap and electronic states. The energy cut-off is 520eV. The screened exchange (sX) method [38] is also implemented to calculate the electron affinity of g-C_3N_4. The cut-off energy is 700eV.

For the larger a-CN_x:H network of 1728 atoms we used the DFTB+ code [39] a semi-empirical DFT code using a basis set of local orbitals. In this case, the system was heated up to 3000K for 100 ps and then quenched to 300K with a cooling rate of 100K/ps. The final structure was then relaxed until the residual force was less than 0.02 eV/Å. The g-CN_x:H retains some hydrogen. It is useful to retain hydrogen for building networks of larger effective size. The hydrogen lowers the atomic coordination at critical vertices, which can be useful for reducing network size during simulations.

3 Results

3.1 Ideal crystalline g-C_3N_4.

The band structure of crystalline g-C_3N_4 can be derived from that of h-BN and thereby from that of graphene. The graphene primitive lattice has two sites. Its band structure consists of σ states within the x,y plane and π states directed along z normal to the x.y plane. At the K point of the zone, the π bands cross over, and at the K point these two bands are localized on the opposite atomic sites.

h-BN consists of the same two atomic sites as graphene, one B and the other N. Its band structure also has σ states lying in the x.y plane and π states lying along the z-axis. But unlike graphene, the π states of h-BN form a minimum direct gap at the K point for the monolayer, where the valence band maximum is pure N-like and the conduction band minimum is pure B like. In the 3D h-BN lattice

(Fig 1), its bands have a slight indirect gap from a valence band maximum at K to a conduction band minimum at M [40].

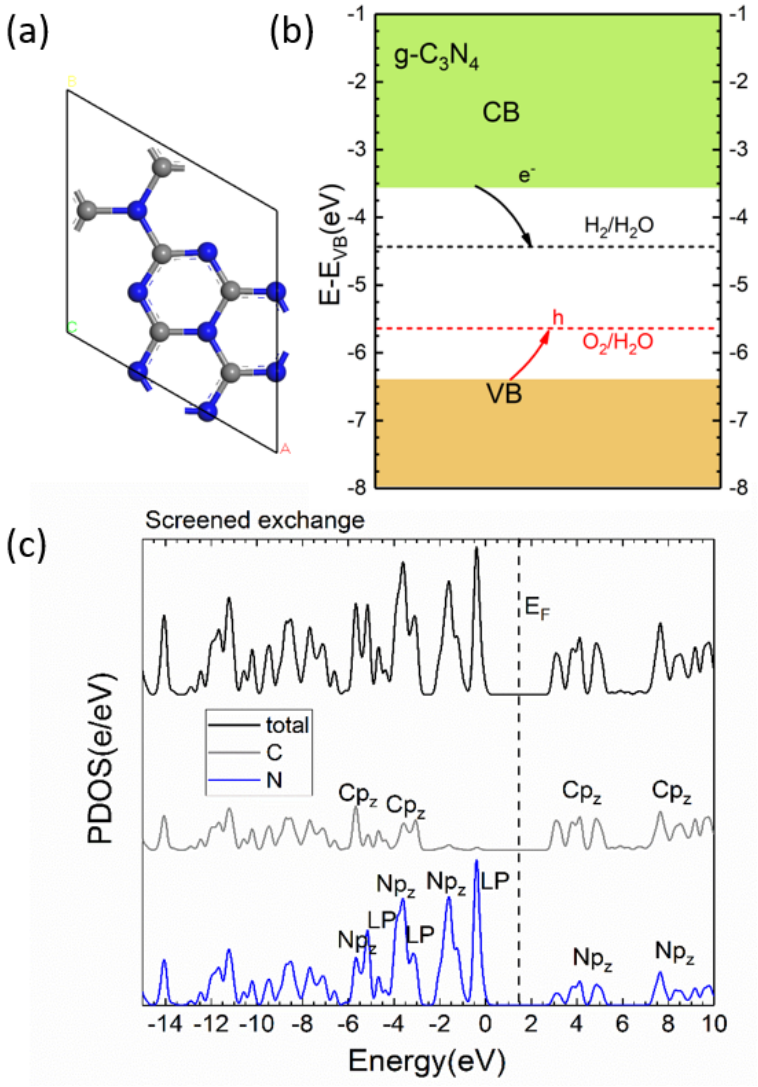

Fig. 1. (a) Atomic structure of melem unit. Blue = N, gray = C. (b) Band gap and electrochemical hydrogen and oxygen evolution levels of water, with respect to the vacuum level (c) Calculated partial density of states of g-C_3N_4 using the SX hybrid functional, with the orbital type indicated at each energy and with energies referred to the valence band maximum..

The g-C_3N_4 lattice can be constructed from this h-BN lattice. Consider the eighteen sites of a 3x3 supercell of a CN lattice based on h-BN, with 1 nitrogen and 1 carbon atom per cell. From this, remove 1 nitrogen atom and 3 adjacent carbon atoms, leaving eight N's and six C's, as in Fig 1(a).

The result of these vacant sites is to create two types of N sites; the two fully bonded 3-fold N, and the six 2-fold bonded N. The 3-fold N sites are like those in h-BN. The 2-fold N sites are a new type; they have the x,y σ states, the z-like π states and also new lone pair states within the x,y plane.

The resulting electronic structure is shown in Fig 1(c). There are a valence and conduction band of σ and σ* states. There is a π-like conduction band of B p_z states with some N p_z admixture. In the valence band, there is an N p_z π-like state, near the valence band (VB) top. At the VB top, there are also non-bonding lone-pair N $p_{x,y}$ states. There are other non-bonding N $p_{x,y}$ states at various lower energies in the VB. Note that while the N $p_{x,y}$ lone pair, and N p_z states can both be pure p-like, charge localization causes the N $p_{x,y}$ state to be slightly above the N p_z states and lie at the VB top.

Finally, by using a supercell with a wider vacuum gap, we can locate the vacuum energy level and reference the band energies to the vacuum energy scale, and thus to the electrochemical scale, as shown in Fig 1(b). The H_2 and O_2 evolution potentials at 4.44 eV and 5.67 eV respectively are seen to lie within the calculated band gap.

Table 1 gives the band energies of g-C_3N_4 by PBE, sX, HSE06, and experiment [18]. The band gap calculated by sX is 2.90 eV, which is close to the experimental value [6].

Table 1. Calculated band gap, ionization potential (IP) and electron affinity (EA) of the carbon nitrides, with reference to Figs. 1,3,4.

	Functional	**Band gap (eV)**	**EA (eV)**	**IP(eV)**
g-C_3N_4	PBE	1.13	3.53	4.66
	sX	3.00	3.37	6.37
	HSE06	2.65	3.33	5.98
	exp	2.7~2.9	-	-
a-CN_x	PBE	0	-	-
	HSE06	0.3	-	-
a-CN_x	PBE	0	4.63	4.63
surface	HSE06	0.35	5.34	5.69

3.2 Random Networks

To obtain a random network of carbon nitride containing a similar bonding configuration to crystalline g-C_3N_4, and containing the local melem structure, we tried a molecular dynamics (MD) annealing process. However, we found that it was difficult to obtain a good a-CN_x structure from standard density functional MD because this resulted in too many like-atom N-N bonds, which makes it difficult to form the melem units. Essentially, the supercell size was too small.

Examining the local bonding in recent glassy carbon networks [30,31], it is clear that they contain mainly two types of defects, 'grain boundaries' of lines of adjacent 5- and 7-fold rings, and arrays of 5-fold rings to supply Gaussian curvature to allow closed curvature [35]. If we obtain a gently wavy layered carbon network, we can then tile its layers with melem units to convert it into a-C_3N_4, with only a minimal density of additional 5-fold rings and like-atom bonds.

Reactive force fields for disordered sp^2 carbon have recently been successful used to generate structures for glassy carbon. It will be possible to convert amorphous glassy carbon structures generated by reactive force fields into a-C_3N_4 networks by tiling.

However, a generalization of such a force field to generate a-CN_x directly has not yet been successful. There are many more bonding configurations for the nitrogens than for the carbons. A more limited version that constrained both C and N sites to sp^2-like configurations would simplify matters but this has not been tried.

Such networks involve many thousands of atoms, If such networks are tried on a smaller scale, it results in many adjacent odd membered rings with ill-defined form. Therefore, in order to get a prompt result, a more indirect route was used, which enforces a preference for sp^2 bonding and 6-fold rings chemically using DFT MD.

We first created an amorphous sp^2 carbon network noting the properties of other recently constructed sp^2 a-C networks [30,31,33,34]. We then substituted some C sites with N with a ratio close to C: N=3:4. We start from a supercell of 300 atoms with random coordination and density of 1.5 g/cm^3. We heat the system to 8000K for a 1ps, to make carbon as amorphous as possible, then cool this down to 300K. From 8000K to 500K, the temperature step is 500K and we run the MD at each temperature for 1ps. Then at 300K, we run the MD for 1ps. We use the canonical ensemble (NVT) to maintain a constant volume and temperature with a time step of 3fs, and using the Nosé-Hoover-Langevin (NHL) thermostat to give the NVT dynamics. To make the MD computationally viable, we use only a Γ point as the cell constant is 14.99Å.

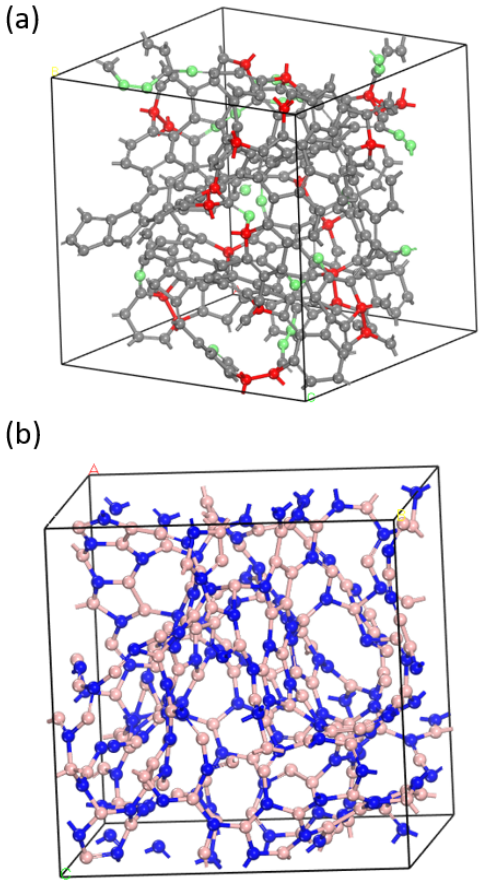

Fig 2(a). The structure of a-C with 300 carbon atoms in a supercell, density is 1.5g/cm^3. 3-fold C = grey, 2-fold C = green, 4-fold C = red. (b) The structure of a-BN with 168 B and 129 N atoms. The density is 1.51g/cm^3 and N = blue, B = pink.

After the annealing process for a-C, we have a structure with appropriate MRO, but with some sp^1 carbon chains. We manually remove any carbon chains and adjust the coordination and relax the structure with constant volume. Finally, we obtain a structure shown in Fig 2(a). The fraction of non-sp^2 carbon is less than 20% (Table 2).

Next, we replace about half of the carbon atoms by boron atoms and the other carbon atoms by nitrogen atoms. This makes an amorphous BN network. We make some adjustments and then relax the structure, to give that seen in Fig 2(b). The ratio B:N is 1.3: 1 and the density is 1.51 g/cm^3.

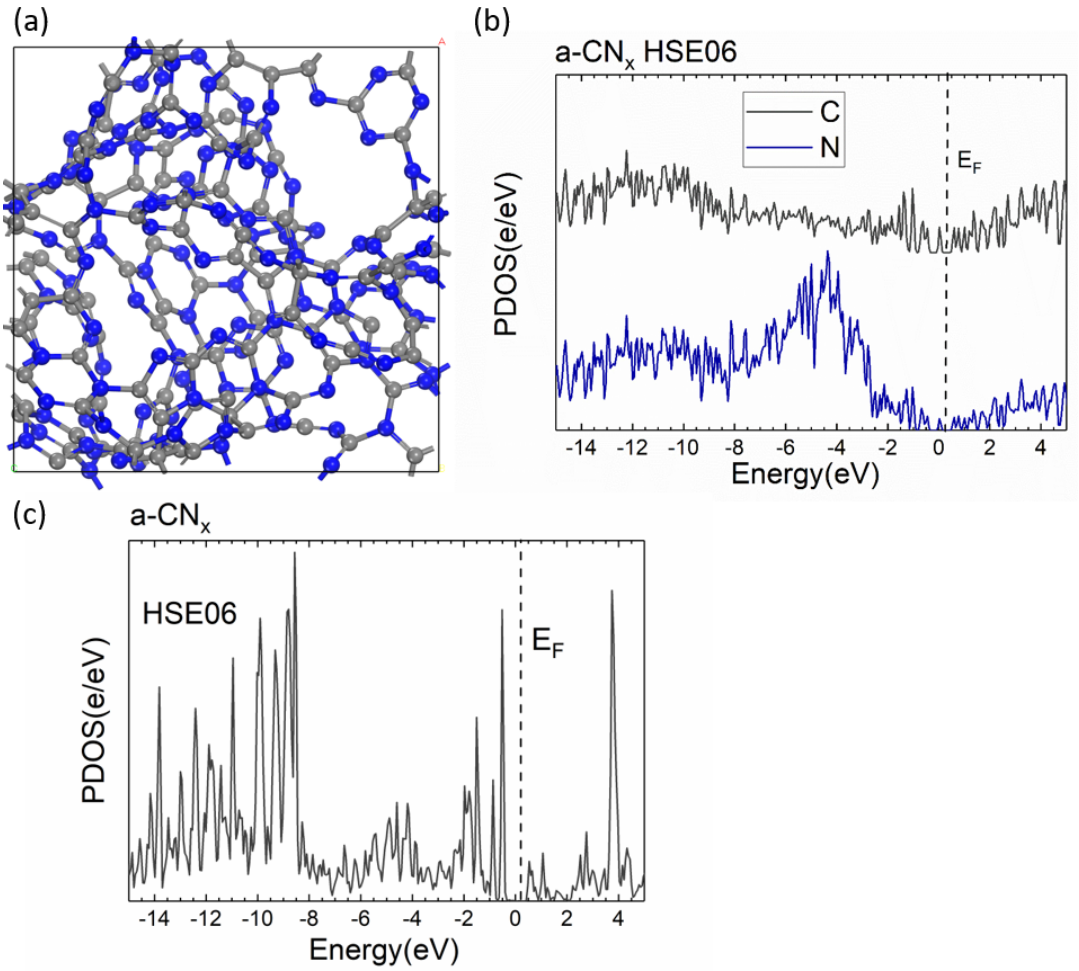

Fig. 3. Graphitic 2D C_3N_4 (a) Its atomic structure, (b) partial density of states (PDOS) calculated by HSE06 functional.(c) local PDOS on pairs of C-C bonds, showing how they create gap states around E_F.

We then substituted all of the boron atoms with carbon atoms and create some vacancies by deleting some of the carbons so that its composition approaches that of C_3N_4. We must then relax the supercell. We fix the atom's fractional coordinate in the supercell and allow the cell size to relax since the C-N bond length is less than the C-C length. We then fix the cell's lattice constant and relax the atom fractional coordinates, in several steps. Between each step, we observe the supercell and try to remove any N-N bonds and carbon chains by removing some of the nitrogen atoms or substituting the nitrogen with carbon, then relaxing the structure again. After two or three cycles of this process, we obtain a network free of N-N bonds and free of sp^1 carbon chains, with most of the carbons 3-fold coordinated, as shown in Fig 3(a). The C and N composition ratio is 1:0.98. Melem type units can be seen in the structure. However, the network has an obvious excess of carbon, leading to C-C bonds.

The total energy of this structure can be compared to that of the crystalline C_3N_4 plus graphene (for the excess carbon sites). This higher energy is found to equal 0.316 eV/atom. This compares to 0.42 eV/atom of the C_{60} molecule [35].

The calculated partial density of states (PDOS) of the C and N sites is shown in Fig. 3(b). The Fermi level is at 0 eV. The PDOS is seen to have only a small band gap within HSE06 (and zero band gap in PBE). This is due to the excessive degree of the disorder. Although the local structure shows the presence of melem units, there are also C-C bonds. The dihedral angle disorder along the C-C bonds causes a closing of the band gap. The upper valence states from -3 to -6 eV are N-rich, consistent with the PDOS of the crystalline lattice, Fig 1(c). The lower CB states have a similar intensity on both C and N sites.

While the network has many melem units, there are also a number of 5-fold rings. These inevitably contain C-C bonds. These bonds give rise to gap states as can be seen in their local PDOS in Fig. 3(c). The typical gap between π and π^* states would be over 3 eV, but this is narrowed by the effect of the rest of the network, and also by the dihedral angle.

Table 2. Number and Percentage (in the column) of atoms with different bonding types in the a-CN_x network.

	2-fold	**3-fold**	**4-fold**
C	18 (14.5%)	98 (79.0%)	8 (6.5%)
N	78 (63.9%)	36 (29.5%)	8 (6.6%)

Table 2 gives the percentage of 2-fold, 3-fold and 4-fold C and N sites. These values compare to the perfect lattice, where the percentages 3-fold C is 100%, and the percentage of 3-fold N is 25% and 2-fold N is 75%, see Fig 2(a). The lattice constant of this g-C_3N_4 is calculated to be 7.16Å by PBE. The C-N bond length is 1.34Å inside the melem hexagonal loop and 1.48Å at the connection of two melems. The C-N bond length in a-CN_x is in the range of 1.30Å to 1.43Å. Thus, the structure of a-CN_x is nearly homogenous while locally it preserves the 3-fold C and 2 or 3-fold N bonding as its crystalline counterpart.

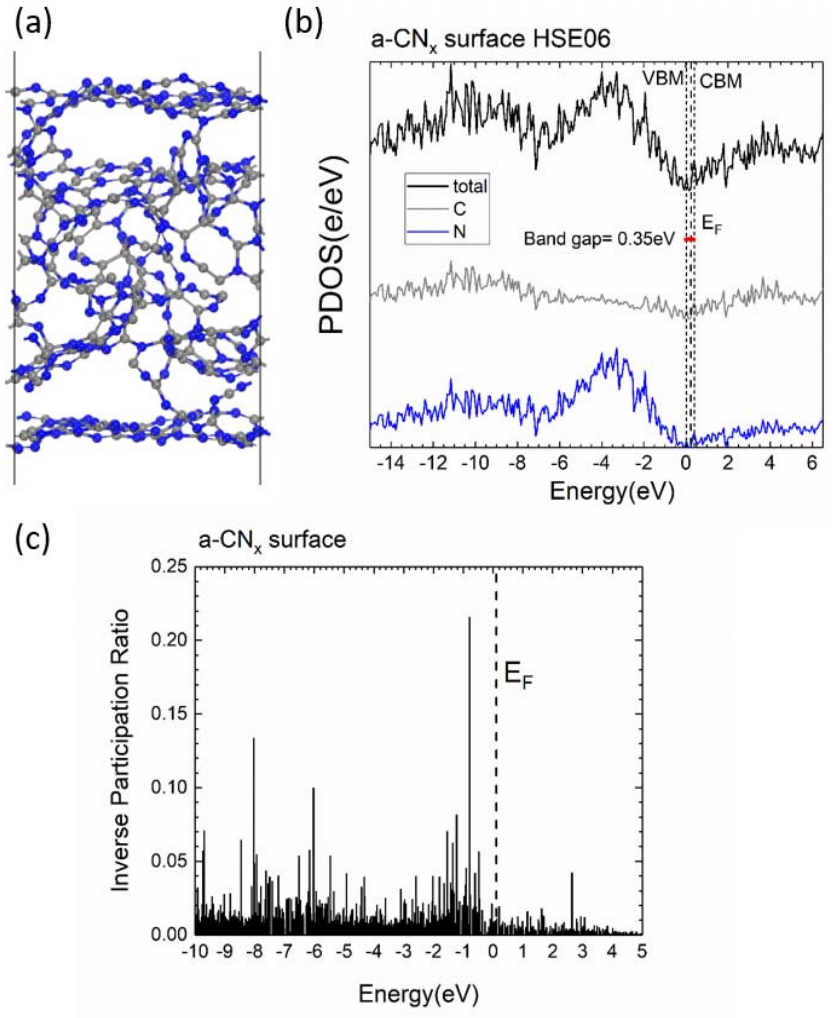

Fig 4. (a) Atomic structure, (b) PDOS (c) and inverse participation ratio of the a-CN_x network with surfaces. The carbon is grey and the nitrogen is blue. The zero reference energy is the Fermi level.

Table 1 shows the calculated band gaps of both carbon nitrides. The results are compatible with experimental measurements. PBE underestimates the band gap but it gives the same electron affinity as the hybrid functional value.

To calculate the electron affinity of the amorphous nitride network, we create a supercell network with a surface, as shown in Fig 4(a). The structure is similar to the bulk a-CN_x network in Fig 3(a) but terminated by a wave-like monolayer of hexagonal carbon nitride with some vacancies and disordered bonds to make it periodic, so that there is no broken bonds. The presence of a vacuum gap in the supercell allows us to define the vacuum potential. Using this as a reference we can calculate the ionization potential and electron affinity as given in Table 1. Fig 4(b) shows the PDOS of this structure. Unfortunately, the band gap is still rather small due to the dihedral angle disorder.

An important factor in disordered networks is the degree of localization of states, defined by the inverse participation ratio (IPR), P. For a state expanded as a complete set of mutually orthogonal localized orbitals, $\psi = \sum_i c_i \phi_i$, where $\sum c_i = 1$, P is given by [19],

$$P = \sum_i c_i^4$$

P measures how localized a state is. For a state localized on a single site, then P=1, while if it distributes equally across N sites, P=1/N. Fig. 4(c) shows the IPR for the network of Fig 4(a). There is strong localization for the upper valence states.

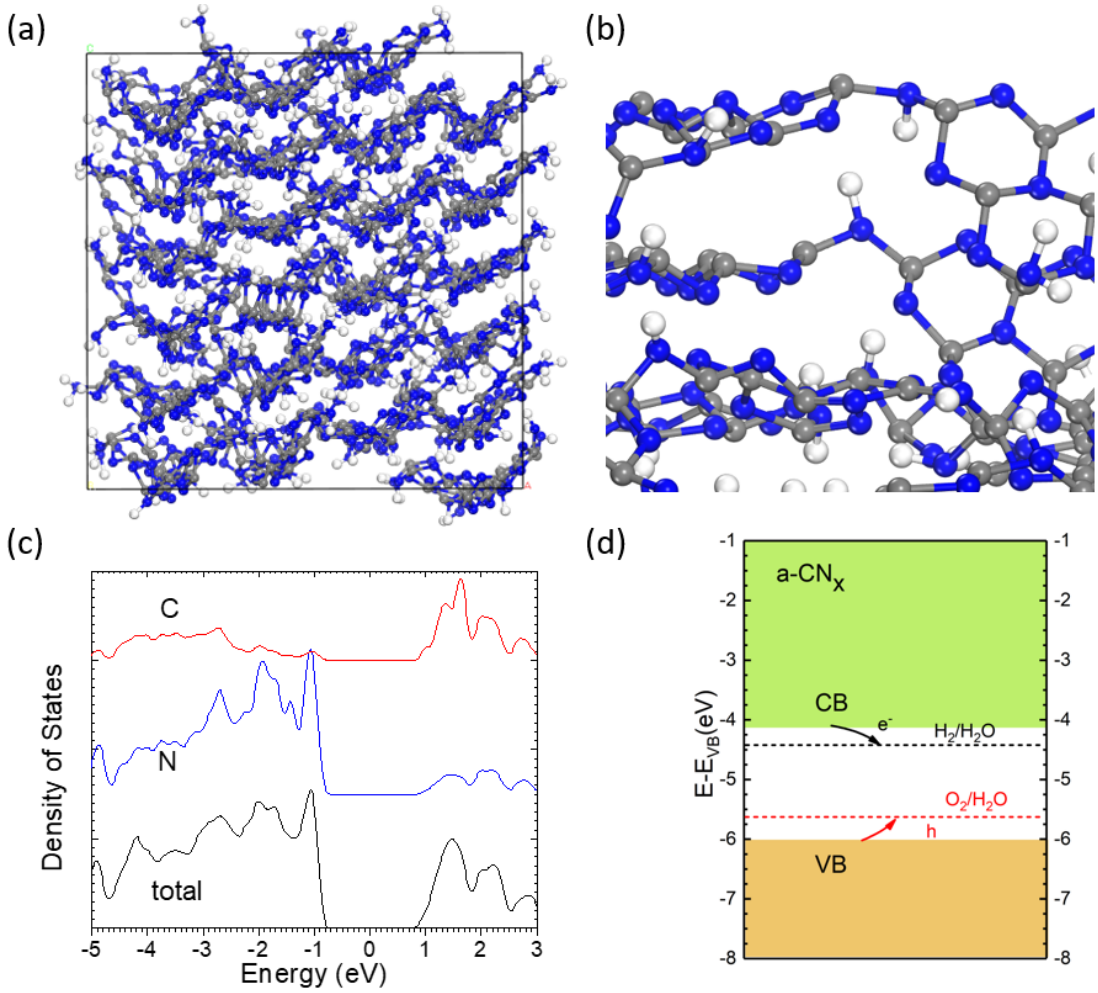

Fig 5. (a) a-CN_x:H network containing a small fraction of hydrogen, (b) a close-up of the network's layer units showing a puckering of adjacent C and N sites, and hydrogen attaching to N sites. (c) the PDOS by HSE06, (d) the band diagram with the water reduction and oxidation levels shown.

Finally, we created an a-CN_x:H network of 1728 atoms with some retained hydrogen atoms. This is subjected to molecular dynamics treatment using the DFTB+ code [39]. The system was heated up to 3000K for 100 ps and then quenched to 300K with a cooling rate of 100K/ps. The final structure was then relaxed until the residual force was less than 0.02 eV/Å. In this case, the network still

retains some layered-like structure but is disordered within each layer, Fig 5(a). The hydrogens allow other types of disorder without creating C-C bonds. They can allow rotations about the trivalent nitrogen junction sites, as seen in the lattices of Pickard [41]. These networks have close to the C:H = 3:4 stoichiometry. A major form of their disorder is an internal puckering of the CN layers, as seen Fig 5(b). This causes a reduction of the band gap to around 1.9 eV, as seen in the calculated PDOS within HSE in Fig 5(c). A similar band gap reduction was found by Kang et al [9]. By using a vacuum gap, we can also set the vacuum reference potential. This results in a band diagram as shown in Fig 5(d), with both the reduction and oxidation potentials lying within the calculated band gap.

Conclusions

We have generated various random networks of amorphous graphitic carbon nitride using a density functional molecular dynamics approach. The random networks contain the melem units and medium range order found in the crystalline phase. The total energy of the random network is 0.32 eV per atom less stable than the crystalline phases, similar to the loss of stability of C_{60}. The in-plane N lone-pair states form the top of the valence band, lying just above the N pπ states. The desnity of states of the amorphous phase has many gap states, which are caused by residual C-C bonds at 5-fold rings and other configurations. Hydrogenated networks have few gap states and a calculated band gap close to the optical gap of 1.9 eV.

Acknowledgments

We acknowledge the support from the Cambridge Center for Carbon Reduction in Chemical Technology (C4T) CREATE programs.

4 REFERENCES

1. A Fujishima, K Honda, Nature 238 (1972) 37
2. V Stevanovic, S Lany, D S Ginley, W Tumas, A Zunger, Phys Chem Chem Phys 16 (2014) 3706
3. P G Moses, C G Van der Walle, App Phys Lett 96 (2010) 021908
4. X Wang, K Maeda, A Thomas, K Takanabe, G Xin, J M Carlsson, K Domen, and M Antonietti. Nat. Mater. **8** (2009) 76.
5. X Chen, Y S Jun, K Takanabe, K Maeda, K Domen, X Fu, M Antonietti, X Wang, Chem. Mater. **21**, (2009) 4093.
6. J H Zhang, X F Chen, K Takanabe, K Maeda, K Domen, J D Epping, X Z Fu, M Antonietti, X C Wang, X. C. Angew. Chem., Int. Ed. **122**, (2010) 451.
7. J Zhang, X Chen, K Takanabe, et al. Angew. Chem. International Edition, **49** (2010) 441.
8. S Yang, Y Gong, J Zhang, L Zhan, L Ma, Z Fang, R Vajtai, X Wang, P M Ajayan, Adv. Mater. **25**, "013) 2452.
9. Y Kang, Y Yang, L C Yin, X D Kang, G Liu, H M Cheng, Adv. Mater. **27** (2015) 4572.
10. P Niu, L C Yin, Y Q Yang, H M Cheng, Adv Mater 26 (2014) 8046
11. K Schwinghammer, M B Mesch, V Duppel, C Ziegler, J Senker, B V Lotsch, J. Am. Chem. Soc. **136** (2014) 1730.
12. Y Xu, M Kraft, R Xu, Chem Soc Rev 45 (2016) 3039
13. J Liu, Y Liu, N Liu, Y Han, X Zhang, H Huang, Y Lifshitz, S T Lee, J Zhong, Z Kang, Science 347 (2015) 970
14. W J Ong, L L Tan, Y H Ng, S T Yong, S P Chai, Chem Rev 116 7(2016) 159
15. J Liu, H Wang, M Antonietti, Chem Soc Rev 45 (2016) 2308
16. W Tu, Y Xu, J J Wang, B W Zhang, T H Zhou, S M Yin, S Y Wu, C M Li, Y Z Huang, Y Zhou, J Robertson, M Kraft, R Xu, ACS Sust Chem & Engin, **5** (2017) 7260.
17. L Luo, M Zhang, P Wang, Y Wang, F Wang, New Journal of Chemistry, **42** (2018) 1087.
18. L Song, T Li, S Zhang, J. Phys. Chem. C, **121** (2016) 293.
19. A Y Liu, M L Cohen, Science 245 (1989) 841; D M Teter, R J Hemley, Science 271 (1996) 53
20. S E Rodil, W I Milne, J Robertson, L M Brown, App Phys Lett 77 (2000) 1458
21. Z J Zhang, S S Fan C M Lieber, App Phys Lett 66 (1995) 3582
22. C W Chen, J Robertson, J Non-Cryst Solids 227-230 (1998) 602
23. F Wooton, K Winer, D Weaire, Phys Rev Lett 54 (1985) 1392
24. D Beeman, J Silverman, R Hynds, M R Anderson, Phys Rev B 30 (1984) 870
25. X Wang, K Ho, Phys Rev Lett 71 (1998) 1184
26. U Stephan, T Frauenheim, P Blaudeck, Phys Rev B 52 (1995) 11837
27. R Haerle, E Riedo, A Pasquarello, Phys Rev B 65 (2002) 045101
28. J Robertson, E P O'Reilly, Phys Rev B 35 (1987) 2946
29. J Robertson, Adv Phys 35 (1986) 317
30. C de Tomas, I Suarez-Martinez, N A Marks, Carbon 109 (2016) 681
31. C deTomas, I Suarze-Martinez, F Vallejos-Burgos, M J Lopez, K Kaneko, N A Marks, Carbon 119 (2017) 1; Appl Phys Lett 112 (2018) 251907
32. T B Shiell, D G McCulloch, D R McKenzie, M R Field, B Haberl, R Boehler, B A Cook, C deTomas, I Suerez-Martinez, N A Marks, J E Bradby, Phys Rev Lett 120 (2018) 215701
33. B Bhattarai, D A Drabold, Carbon 115 (2017) 532
34. B Bhattarai, A Panday, D A Drabold, Carbon 131 (2018) 168
35. T Lenosky, X Gonze, M Teter, V Elser, Nature 355 (1992) 333
36. S. J. Clark, M. D. Segall, C. J. Pickard, P. J. Hasnip, M. J. Probert, K. Refson, and M. C. Payne, Z. Kristallogr. **220** (2005) 567 .
37. J. Heyd, G. E. Scuseria, and M. Ernzerhof, J. Chem. Phys. **118** (2003) 8207.
38. S. J. Clark and J. Robertson, Phys. Rev. B **82** (2010) 085208.
39. B Aradi, B Hourahine, T Frauenheim, J Phys Chem A 111 (2007) 5678
40. B Arnaud, S Lebegue, P Rabiller, M Alouani, Phys Rev Lett 96 (2006) 026402
41. C J Pickard, A Salamat, M J Bojdys, R J Needs, P F McMillan, Phys Rev B 94 (2016) 094104